The Seventh International Colloquium on Bluff Body Aerodynamics and Applications (BBAA7)
Shanghai, China; September 2-6, 2012

Cross Spectra of Wind Pressures on Domed Roofs in Boundary Layer Wind Tunnel

Yuan-Lung Lo [a], Jun Kanda [b]

[a] *Tamkang University, Tansui, New Taipei City, Taiwan*
[b] *Nihon University, Chiyoda, Tokyo, Japan*

ABSTRACT: This research intends to investigate the cross spectrum characteristics of wind pressure fluctuations on the surface along the meridian of domed roofs under turbulent wind flows. Wind pressure experiments of domed roofs are conducted considering two roof curvatures and three heights of side walls. From the experimental results, various distribution types of co-coherences are examined and the traditional exponential decaying form is shown insufficient to approximate the general characteristics of co-coherences. By combining the proposed models by Uematsu et al ([1]) and Kanda et al ([2]) and also a phase shift parameter included, the approximation model is then improved to represent the observed coherences generally.

KEYWORDS: Domed roof, Roof curvature, Wind pressure fluctuation, Cross spectrum, Root-coherence, Phase distribution

1 INTRODUCTION

The curved geometric appearance makes the estimation of wind loads a difficult task for wind resistant design of a dome structure. Wind pressure distributions on the roof become more complicated due to the occurrence of separation and the formation of wake. Researches regarding the curved roofs or domed roofs have been investigated for the past two decades, typically the hemispherical domed roofs. Taylor ([3]) measured mean and R.M.S. pressures on the surfaces of domed roofs. Ogawa et al ([4]) investigated mean and R.M.S. wind pressures and spectrum characteristics of domed roofs with three height span ratios in one laminar and two turbulent boundary layer flows. Uematsu et al ([1]) proposed a computer-assisted wind load evaluation system for the design of roof cladding of hemispherical domes. Cheng et al ([5]) conducted a series of wind tunnel tests to investigate the effects of Reynolds number on the aerodynamic characteristics of hemispherical dome in smooth and turbulent boundary layer flows.

However, discussions on cross spectra of wind pressures on domed roofs have not been made sufficiently and usually only one uniform exponential decaying distribution is assumed for all cross spectra on one specific dome roof (Hongo [6]). In this research, wind pressure characteristics and distribution types of cross spectra are examined and the effects of roof curvatures and height-span ratios are investigated. A general approximation model is then proposed to achieve better agreement of approximation, especially for the cross spectra near the separation point.

2 SIMULATED TURBULENT WIND FLOW

2.1 Experimental setting of simulation of turbulent flow and acrylic domed models

The indoor closed-circuit Eiffel type wind tunnel simulator in University of Tokyo is used to generate turbulent boundary layer flow for the wind pressure experiments in this research. The geometric size of the working cross section is 1.8m×1.8m×15.6m. Turbulent wind flow is simu-

lated by the arrangement of spires and roughness blocks to fit the urban terrain (terrain IV, power law index $\alpha = 0.27$) specified in AIJ recommendation ([7]). Wind speed at boundary layer height is 11.00m/sec (U_g). I-type hot wire probe is used for measurements of wind profiles and fluctuating wind speeds. Figure 1 shows the normalized mean wind profile and the turbulence intensity profile compared to the distribution for terrain IV in AIJ model.

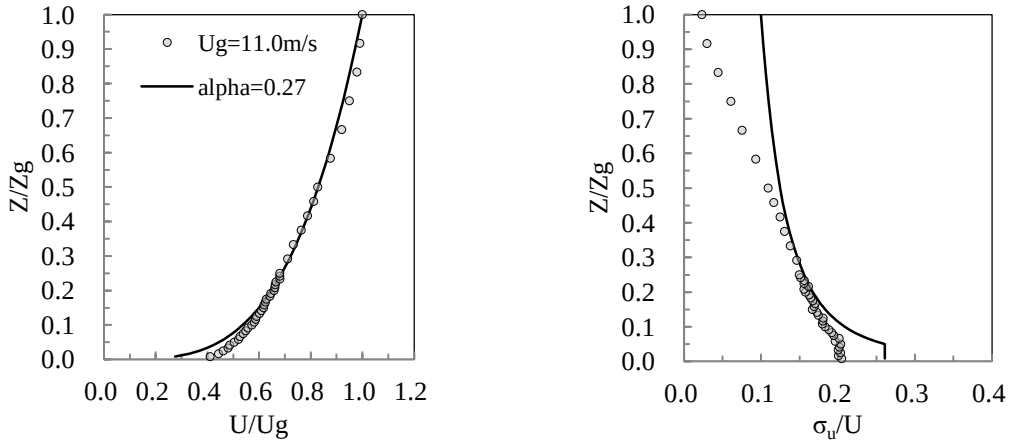

(a) Mean wind speed profile (b) Turbulence intensity profile

Figure 1 Normalized profiles of mean wind speeds and turbulence intensities

Wind pressure measurements in this research are conducted by the micro-pressure measuring system manufactured by Kyowa Electronic Instruments Co., Ltd. Fluctuating pressures on the surface of domed models are simultaneously recorded and then digitalized for saving and further analyses. Each domed model is composed of two acrylic models, a roof model and a cylinder model. The geometric definitions of a testing model are shown in Figure 2. The span of the roof models is fixed to be 300mm. Vinyl tubes for pressure measurements are arranged to taps along the meridian parallel to the wind direction. Two roof curvatures and three side wall heights are selected to understand generally the geometric effect. Table 1 lists the nomenclature of domed models in this research. 1/400 is assumed for the length scale ratio, 1/70 for the time scale and 1/5.7 for the wind speed scale ratio. Figure 3 shows the coordinates inside the wind tunnel.

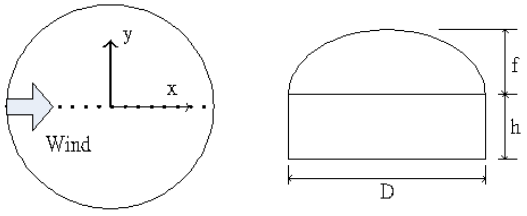

Figure 2 Geometric definitions of a domed model

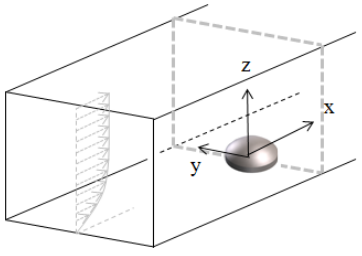

Figure 3 Coordinates inside wind tunnel

Table 1 Nomenclature of domed models

D = 300mm		f/D (roof height to span) 0.2	0.5
h/D (cylinder height to span)	0.0	C0	F0
	0.2	C2	F2
	0.5	C5	F5

Reynolds numbers of domed models are defined as the hemispherical domes by the roof span, mean wind speed at model height, air density, and viscosity constant ([1]). Mean wind speed at the height of the models is varying from 5.1m/sec to 7.5m/sec. The range of Reynolds numbers is 1.1×10^5~1.6×10^5. According to Cheng et al ([5]), when the turbulence intensity of approaching wind is high enough (>18%~20%), the Reynolds number effect is less significant when it is larger than 10^5.

2.2 Basic characteristics of fluctuating wind speeds

Power spectra of fluctuating wind speeds along the vertical profile are examined. Two examples at z=60mm and 150mm are plotted with Karman's model in Figure 4 to show fairly good agreements. σ_u represents standard deviation of fluctuating wind speeds; $S_u(n)$ represents the power spectral density; n represents the frequency; L_{ux} represents the length scale in the along-wind direction; U_z represents the mean wind speed at elevation z.

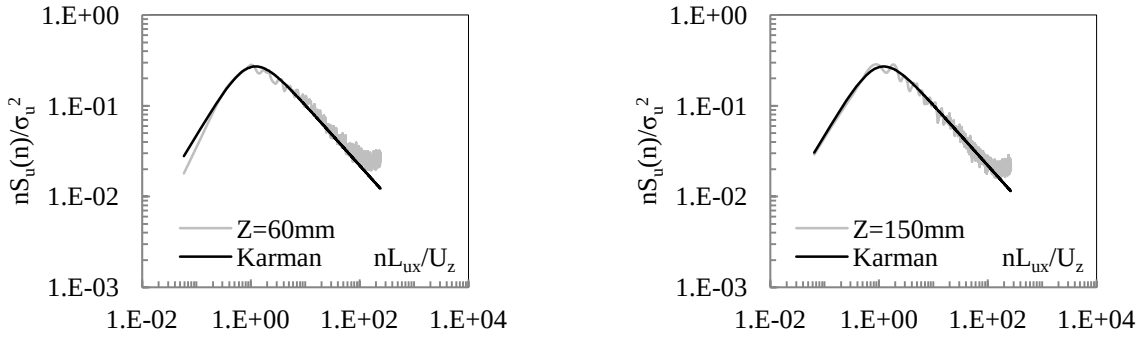

(a) Z = 60mm (b) Z = 150mm

Figure 4 Power spectra of fluctuating wind speeds at elevations

For fluctuating wind speeds at any two points, the cross spectrum of two fluctuating wind speeds or pressures between two points can be defined as follows.

$$S_{12}(r,n)=S_{12}^{C}(r,n)+iS_{12}^{Q}(r,n) \tag{1}$$

where r represents the distance between point 1 and 2; $S_{12}^{C}(r,n)$ represents the real part, co-spectrum; and $S_{12}^{Q}(r,n)$ represents the imaginary part, quadrature-spectrum. Coherence functions can be further defined as the following equations, equation (2) for co-coherence, (3) for root-coherence, and (4) for phase function.

$$C_{12}(r,n)=\frac{S_{12}^{C}(r,n)}{\sqrt{S_1(n)\cdot S_2(n)}} \tag{2}$$

$$R_{12}(r,n)=\frac{\left|S_{12}^{C}(r,n)+iS_{12}^{Q}(r,n)\right|}{\sqrt{S_1(n)\cdot S_2(n)}} \tag{3}$$

$$\theta_{12}(r,n)=\tan^{-1}\left(\frac{S_{12}^{Q}(r,n)}{S_{12}^{C}(r,n)}\right) \tag{4}$$

where $S_1(n)$, $S_2(n)$ represent power spectrum of fluctuating wind speeds at point 1, 2.

Davenport ([8]) proposed a model for root-coherence between two points at different elevations. As the distance increases, the coherence decreases.

$$R_{12}(r_z, n) = \exp\left(-k_z \frac{r_z \cdot n}{\overline{U}_{10}}\right) \tag{5}$$

where k_z is the decay factor around 7.7 and r_z is the vertical distance of two points; U_{10} is the mean wind speed at 10 meter height. Kanda et al ([2]) investigated the variation of coherence near zero frequency and then proposed a modified frequency term for a better modeling. Equation (6) represents the modified co-coherence model.

$$R_{12}(r_y, r_z, n) = \exp\left(-\frac{\sqrt{k_{1y}^2(z_m)\cdot r_y^2 + k_{1z}^2(z_m)\cdot r_z^2}}{\overline{U}_{10}} \cdot n^*\right) \tag{6}$$

$$n^* = \sqrt{\left(\frac{\overline{U}_{10}}{k_2 L(z_m)}\right)^2 + n^2}$$

$$k_{1y}(z_m) = k_y(10)\cdot\left(\frac{z_m}{10}\right)^{-\alpha_{Dy}} = 7.0\left(\frac{10}{z_G}\right)^{-\alpha_{Dy}+\alpha}\left(\frac{z_m}{10}\right)^{-\alpha_{Dy}}$$

$$k_{1z}(z_m) = k_z(10)\cdot\left(\frac{z_m}{10}\right)^{-\alpha_{Dz}} = 6.0\left(\frac{10}{z_G}\right)^{-\alpha_{Dz}+\alpha}\left(\frac{z_m}{10}\right)^{-\alpha_{Dz}}$$

$$\alpha_{Dy} = \alpha_{Dz} = 0.3 + \frac{\alpha}{2}$$

where the subscript, m, represents the geometric average of two points. L(z) is length constant; k_1 and k_2 are the decay factors determining the decaying tendency and the root-coherence value at zero frequency. Co-coherences of two fluctuating wind speeds vertically or horizontally are calculated and compared with root-coherence models of (5) and (6) to verify the consistent characteristics of the simulated turbulent wind flow. Figure 5 and Figure 6 respectively show two cases of vertical co-coherences and two cases of horizontal co-coherences. The coordinates of two points are indicated as Figure 3. It is indicated that Kanda's model provides both better fittings at zero frequency and the whole tendency. It is also known that the decay factor increases with the distance of two points increases since the coherence become weaker. The decay factors are estimated 9.8 and 12.9 in Figure 5(a) and 5(b); 8.8 and 16 in Figure 6(a) and 6(b).

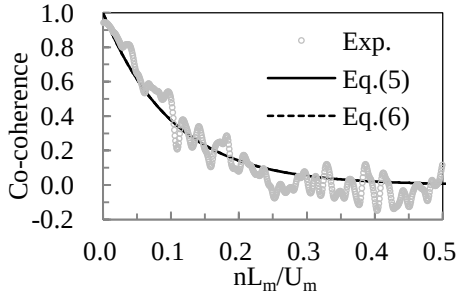

(a) $y_1=y_2=0$; $z_1=60$mm, $z_2=30$mm

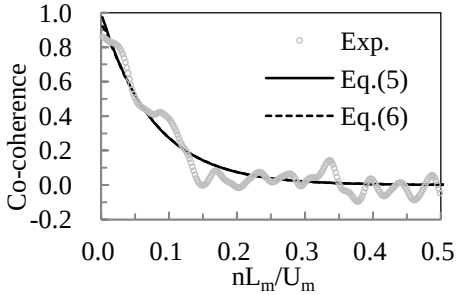

(a) $y_1=y_2=0$; $z_1=150$mm, $z_2=60$mm

Figure 5 Vertical co-coherences compared with equation (5) and (6)

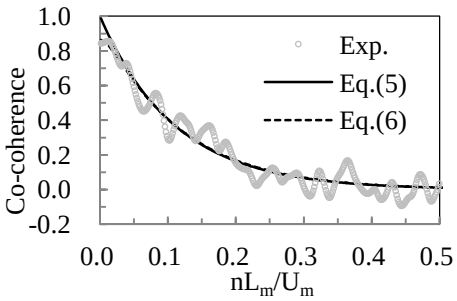

(a) y_1=0, y_2=50mm; z_1=z_2=30mm

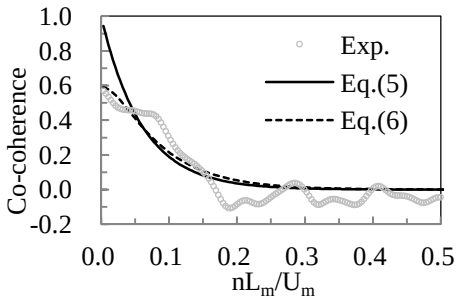

(a) y_1=0, y_2=150mm; z_1=z_2=90mm

Figure 6 Horizontal co-coherences compared with equation (5) and (6)

3 CHARACTERISTICS OF FLUCTUATING WIND PRESSURES

3.1 Distributions of wind pressure coefficients

Wind pressure measurements of domed models are conducted under the simulated turbulent wind flow mentioned in the previous section. The sampling rate is 1000Hz for a 2 minute record. According to the time scale ratio assumed, 14 segments are averaged for the observation results. Moving averaging is also conducted by 1 second average. The definitions of mean and R.M.S. wind pressure coefficients are as follows.

$$C_{p,i} = \frac{p_i - p_s}{q_H} \tag{7}$$

$$C_{p,mean} = \frac{1}{N}\sum_{i=1}^{N} C_{p,i} \tag{8}$$

$$C_{p,rms} = \sqrt{\frac{1}{N}\sum_{i=1}^{N}\left(C_{p,i} - C_{p,mean}\right)^2} \tag{9}$$

$$q_H = \frac{1}{2}\rho\overline{U}_H^2 \tag{10}$$

where p_i and p_s represent instantaneous wind pressure at the i-th point and reference static pressure at model heights. ρ is air density. U_H is the mean wind speed at model heights.

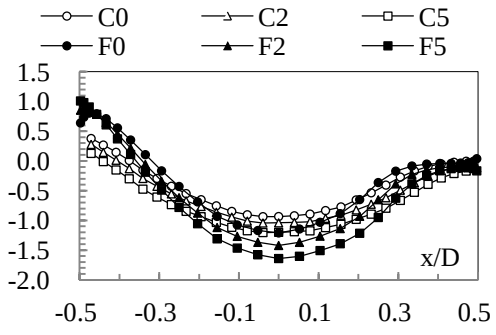

Figure 7 Distributions of mean wind pressure coefficients, $C_{p,mean}$

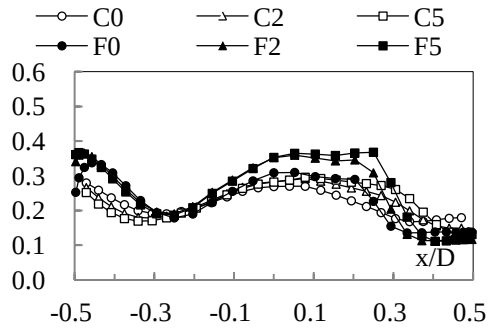

Figure 8 Distributions of R.M.S. wind pressure coefficients, $C_{p,rms}$

Pressure coefficients are plotted in Figure 7 and 8 with respect to f/D and h/D for the mean and RMS respectively to indicate the effects caused by roof curvature and the side wall height. Wind pressures along the meridian can be roughly divided as the windward region, the apex region, and the leeward region. Positive mean wind pressure coefficients can be expected since wind pressure fluctuations in the windward region are mostly affected by the approaching wind. As the flow moves downstream, a thin shear boundary layer forms along the roof surface and negative mean wind pressures are generally distributed in the apex region and leeward region. The apex region and the leeward region are divided by the occurrence of flow separation. Maximum negative pressures can be observed in the apex region. Small mean and R.M.S. coefficients in the leeward region are also indicated. To clarify the wind flow changes on the roof surface, the correlation coefficients between any two neighboring taps are calculated to show the three zones with different patterns as Figure 9.

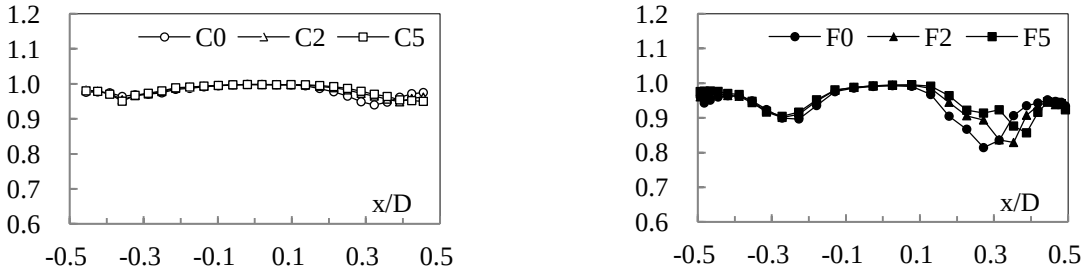

(a) f/D=0.2 models (b) f/D=0.5 models

Figure 9 Distributions of correlation coefficients between two neighboring vinyl tubes

As shown in Figure 9, relatively lower correlation coefficients are observed whenever the wind flow changes. For f/D=0.2 models, the range of the apex region is larger than that for f/D=0.5 models. However, three regions can be more clearly distinguished in those models with higher roof curvatures. It is also indicated that the increase of side wall height slightly pushes the separation point downstream. The three regions can also be named as “windward zone”, “separation zone” and “wake zone” according to the dominant characteristics in each region. Such zoning concept is further used for demonstrating various distribution types of spectrum characteristics in the next two sections. Table 2 lists the channel numbers in each zone/region (zone, hereafter) based on the observations results in this research.

Table 2 Identified channel numbers in three zones based on experimental results

Domed model		Windward zone	Separation zone	Wake zone
f/D=0.2	C0	1~4	5~21	22~27
	C2	1~4	5~24	25~27
	C5	1~4	5~25	26~27
f/D=0.5	F0	1~8	9~20	21~29
	F2	1~8	9~20	21~29
	F5	1~8	9~21	22~29

3.2 Power spectrum characteristics of along the meridian of domed roofs

Power spectrum characteristics of fluctuating wind pressures have been discussed in many publications. Ogawa et al ([4]) proposed fitted parameters for power spectra in three domed models

with different roof curvatures. Qiu et al ([8]) proposed typical power spectra for Gaussian and non-Gaussian zones and weighting factors to approximate power spectra along the meridian. Lo ([9]) then applied the similar idea to find typical power spectra in three zones and provided the fitted parameters of typical power spectra with respect to f/D and h/D for a database work.

Figure 10 shows the power spectra in F0 model to illustrate the dominant characteristics in each zone. The distribution shape of power spectral densities gradually varies from upstream to downstream. Three distinct zones can clearly be identified by several obvious features. For the power spectra in the windward zone, the distribution shape is similar to that of approaching wind speeds. When wind flow moves to the separation zone, a hump at lower frequency appears because of the formation of the thin shear boundary layer. After the occurrence of separation, turbulence energy is dominated by the component resulted from the thin shear boundary and the component resulted from the wake. Two humps are characteristically observed in the wake zone.

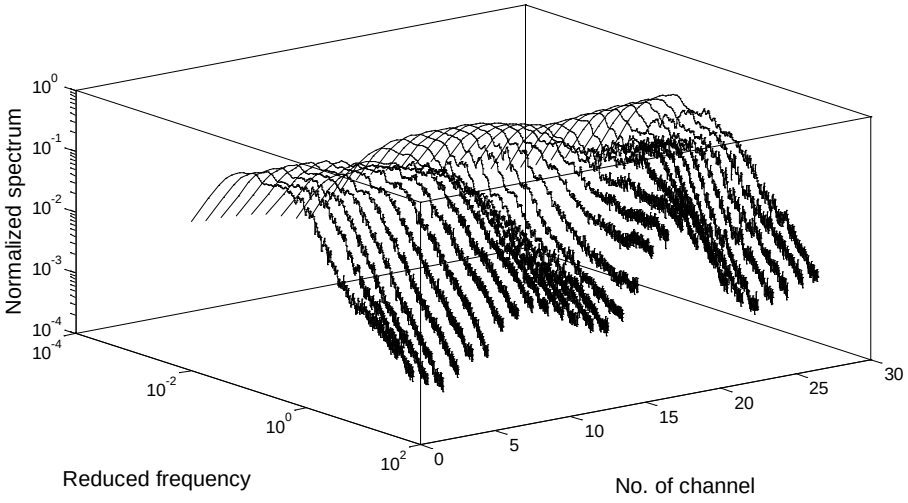

Figure 10 Power spectra along the meridian of F0 model with respect to channel numbers

3.3 Cross spectral characteristics of along the meridian of domed roofs

Cross spectral characteristics of two fluctuating wind pressures can also be examined by co-coherences, root-coherences, and phases, which are defined by equations (2) ~ (4). As discussed in the previous sections, it is clearly noted that each zone contains its specific dominant features in the distributions of wind pressure coefficients and power spectra. Based on the same zoning concept, cross spectra are examined within one zone and across two zones. Typical domed models, C0 model and F0 model, are selected for demonstrating various distribution types of co-coherences in Figure 11.

For co-coherences of two fluctuating wind pressures within the windward zone, a consistent decaying distribution is generally observed. The co-coherence values at zero frequency decrease as the distances between two points increase. It is also indicated that roof curvature results in less significant effect. Within the separation zone, co-coherences are observed to decay quicker with increasing roof curvature and the distance. Within the wake zone, co-coherences remain almost consistent as distance or roof curvature varies. For the co-coherences across the windward zone and separation zone, it is interesting to observe two different patterns when the distance of two points across the apex of the domed model or not. The co-coherence value at zero frequency is negative when the distance across the apex. A clear hump is indicated around reduced frequency

equals 0.1, where a hump can also be pointed out in the distributions of power spectra in the separation zone at lower reduced frequency range. For the co-coherences across the separation zone and wake zone, dramatic decaying is generally observed, especially the cases with larger roof curvature. Low and almost unvaried co-coherences are observed when the distance across the windward zone and the wake zone.

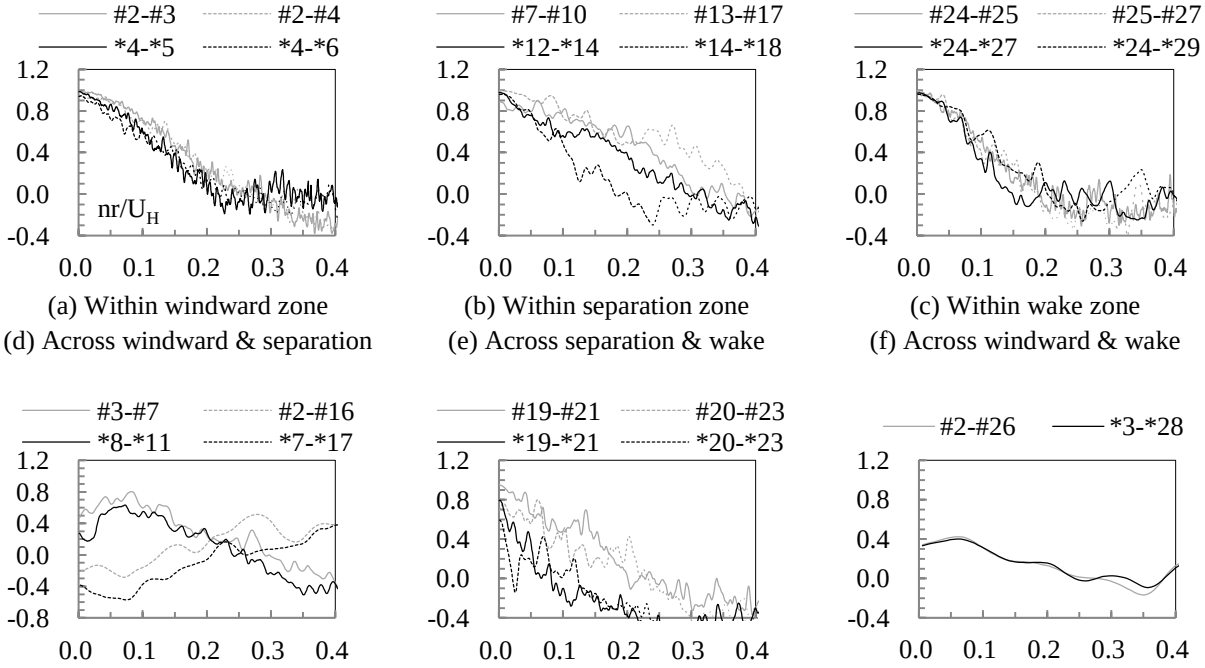

(a) Within windward zone (b) Within separation zone (c) Within wake zone

(d) Across windward & separation (e) Across separation & wake (f) Across windward & wake

Figure 11 Co-coherences within one zone and across two zones (#: C0 model, *: F0 model)

It is summarized from the aforementioned observations that several features should be focused once the approximation of co-coherence is considered: (1) decaying tendency; (2) co-coherence value at zero frequency; (3) the hump at low reduced frequency corresponding to the dominant power spectrum characteristics in the separation zone; (4) negative co-coherence value when the distance of two points across the windward zone and the separation zone, especially two points are at the upstream side and downstream side of the apex respectively.

4 APPROXIMATION MODELS OF CO-COHERENCES

Different from approximation of fluctuating wind speeds, co-coherences of wind pressures cannot be conveniently replaced by root-coherence and described by Davenport's or Kanda's model. In order to generally approximate the features shown in Figure 11, a formula is proposed by representing first root-coherence and phase separately and then combining by the following equation.

$$C_{p,12}(n) = R_{p,12}(n) \cdot e^{i\theta_{p,12}(n)} \tag{11}$$

where $C_{p,12}(n)$, $R_{p,12}(n)$, and $\theta_{p,12}(n)$ represent co-coherence, root-coherence, and phase of two pressures respectively. Ogawa et al ([4]) and Uematsu et al ([1]) ignore the imaginary part of phase and rewrite (11) as (12):

$$C_{p,12}(n) = R_{p,12}(n) \cdot \cos\left(\theta_{p,12}(n)\right) \tag{12}$$

To satisfy the observations of decaying tendency of co-coherence and the value at zero frequency, Kanda's model is slightly modified and substituted to equation (12) for approximating the root-coherence part. Further, to satisfy the hump observed at lower frequency ranges and two opposite patterns shown in Figure 11(d), two parameters are proposed for better approximation agreement. Equation (12) can then be re-written as follows.

$$C_{p,12}(r,n) = \exp\left(-\frac{\sqrt{k_1^2 r^2}}{D} \cdot n^*\right) \cdot \cos\left(2\pi \cdot k_t \cdot \left|\frac{n \cdot r}{\overline{U}_H} - \hat{n}_{cr}\right| - d\theta\right)$$
$$n^* = \sqrt{1 + \left(\frac{n \cdot D}{k_2 \overline{U}_H}\right)^2} - \hat{n}_{st} \tag{13}$$

where k_1 and k_2 are decay factors determining the decaying tendency and the root-coherence value at zero frequency; k_t is a slope constant of the phase and $d\theta$ is a shift constant of phase at zero frequency. $\hat{n}_{cr}$ is the observed dominant reduced frequency of power spectra in the separation zone. $\hat{n}_{cr}$ is around 0.08~0.1 in this research and assumed 0.1 in general. For the co-coherences not across the windward zone and separation zone, $\hat{n}_{cr}$ and $d\theta$ can be assumed zero simply.

Approximation of co-coherences of F0 model shown in Figure 11 are conducted and plotted in Figure 12. Fairly good agreement of approximation is achieved by the improved model of equation (13) rather than the exponentially decaying model. Observed features of co-coherences can be satisfied by providing two more parameters, $\hat{n}_{cr}$ and $d\theta$. The fitted parameters in Figure 12 are listed in Table 3 to indicate that only one unique distribution of co-coherence is insufficient for describing the spectrum characteristics, especially integration of wind loads is conducted among certain surface where the separation of wind flow occurs.

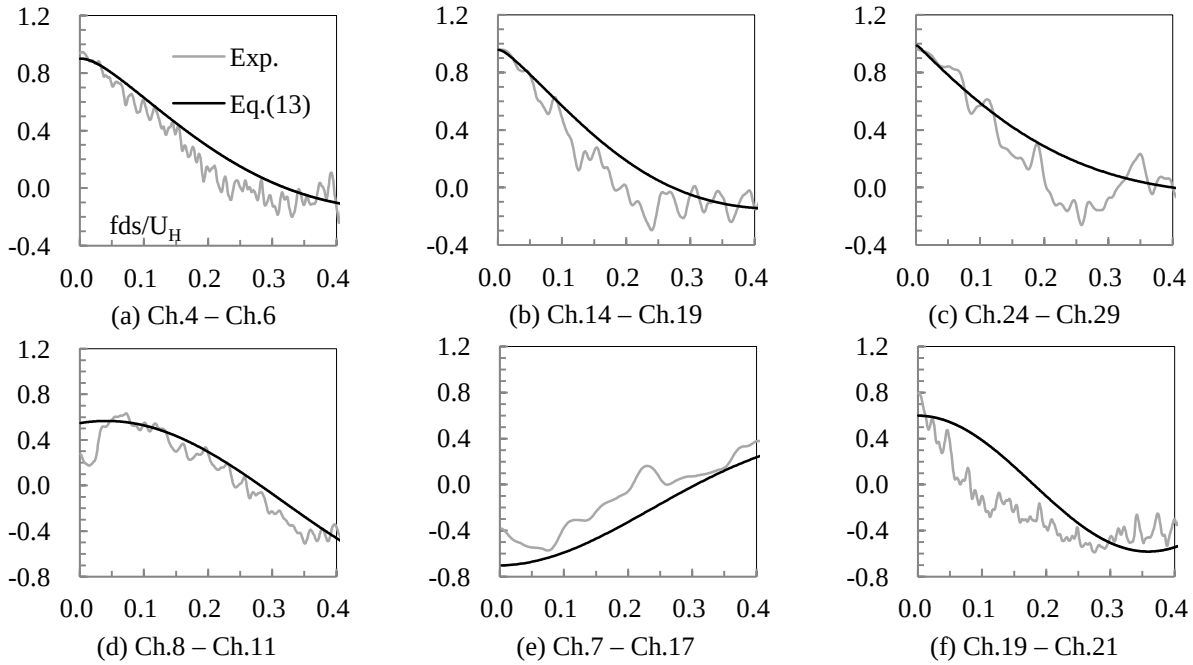

Figure 12 Approximation results of co-coherences in F0 models

Table 3 Fitted parameters of co-coherences in Figure 12 based on equation (13)

	k_1/k_2	k_t	n_{cr}	$d\theta$
Ch.4 – Ch.6	3.24	0.78	0.00	0.00
Ch.14 – Ch.19	3.88	0.92	0.00	0.00
Ch.24 – Ch.29	4.52	0.62	0.00	0.00
Ch.8 – Ch.11	0.56	0.86	0.10	-0.42
Ch.7 – Ch.17	1.48	0.43	0.10	2.61
Ch.19 – Ch.21	0.48	1.39	0.00	0.00

5 CONCLUSIONS

In this research, distribution types of co-coherences were examined and an improved approximation model was proposed by adding two more parameters considering the dominant characteristics of power spectrum and the phase shift when positive pressures convert to significant negative pressures. From the fitted parameters of the proposed model and the approximation results, it is clearly shown that only one unique exponential decaying term is insufficient to represent various coherence features of fluctuating wind pressures on the domed roofs. And it may be considered desirable for integrating wind loads to provide a general co-coherence form based on the zoning concept of wind flow changes.

ACKNOWLEDGEMENTS

Kajima Foundation is acknowledged for its financial support to the wind tunnel experiment in this research. Kyowa Electronic Instruments Co., Ltd. is also acknowledged due to its technological assistance on wind pressure measurement maintenance.

REFERENCES

1 Y. Uematsu, R. Tsuruishi, Wind load evaluation system for the design of roof cladding of spherical domes, J. Ind. Aerodyn., 96 (2008), 2054-2066.

2 J. Kanda, R. Royles, Further consideration of the height dependence of root-coherence in the natural wind, Building and Environment, 13 (1978), 175-184.

3 T. J. Taylor, Wind pressures on a hemispherical dome, J. Ind. Aerodyn., 40 (1991), 199-213.

4 T. Ogawa, M. Nakayama, S. Murayama, Y. Sasaki, Characteristics of wind pressures on basic structures with curved surfaces and their response in turbulent flow, J. Ind. Aerodyn., 38 (1991), 427-438.

5 C. M. Cheng, C. L. Fu, Characteristics of wind loads on a hemispherical dome in smooth flow and turbulent boundary layer flow, J. Ind. Aerodyn., 98 (2010), 328-344.

6 T. Hongo, Experimental studies of fluctuating wind pressures on dome-like roofs, PhD thesis (in Japanese), 1995.

7 Architecture of Institute of Japan, Recommendations for loads on buildings (2004), Maruzen Co., Ltd., 2004.

8 Y. Qiu, Y. Sun, Y. Wu, Power spectra of fluctuating wind pressures on spherical domes, Proceedings of 13th International Conference on Wind Engineering, Amsterdam, 2011.

9 Y. Lo, Characteristics of wind pressure fluctuations on dome-like structures, PhD thesis, 2012.